Available online at www.sciencedirect.com
ScienceDirect
International Journal of Heat and Mass Transfer 50 (2007) 4371–4386
International Journal of HEAT and MASS TRANSFER
www.elsevier.com/locate/ijhmt

# Modelling the pyrolysis of wet wood – I. Three-dimensional formulation and analysis

R.K.K. Yuen [a], G.H. Yeoh [b,*], G. de Vahl Davis [c], E. Leonardi [c]

[a] Department of Building and Construction, City University of Hong Kong, Tat Chee Avenue, Kowloon, Hong Kong
[b] Australian Nuclear Science and Technology Organisation (ANSTO), B40, PMB 1, Menai NSW 2234, Australia
[c] School of Mechanical and Manufacturing Engineering, University of New South Wales, Sydney NSW 2052, Australia

Received 24 March 2006; received in revised form 6 January 2007
Available online 27 March 2007

**Abstract**

A three-dimensional mathematical model for the pyrolysis of wet wood is developed with detailed consideration of moisture evaporation, anisotropic and variable properties, and pressure driven internal convection of gases. Multiple competing reactions are formulated; a single first-order Arrhenius reaction is however applied herein. Transient pyrolysis of a beech wood cube with different initial moisture contents is investigated under various furnace temperatures. Influences of anisotropic properties due to the grain structure on heat and mass transfers are discussed. This model serves as a precursor for Part II: Simulation of piloted ignition of wood in a cone calorimeter of this two-part study.


*Keywords:* Pyrolysis; Wet wood; Evaporation of moisture; Anisotropic properties

## 1. Introduction

The phenomenological understanding of fires in buildings and their associated hazards has deepened considerably over the last decade. This precedence is driven by the dramatic shift from the engineering application of correlation-based methods such as zone methods to filtered discrete solution equations by numerical techniques such as the computational fluid dynamics (CFD) approach. Such transformation is already in progress in building codes, regulations and standards with the gradual movement away from the usual prescriptive-based to more performance-based methodologies. Fire engineers are now given the freedom to employ innovative design, with the aim of more efficient use of space, building materials, and a more cost-effective design, to solve fire-related problems.

The thermal degradation of lignocellulosic fuels is a process of significant interest in the fields of fixed-bed thermochemical biomass conversion and fire safety science. Di Blasi [1] has compared various model predictions employing the semi-global mechanisms, which accounted the formation char, tar and gas, against the primary pyrolysis of cellulose and biomass under chemical reaction control. Because of the complex chemical nature, there is a clear indication that more in-depth study is still required to better comprehend the degradation kinetics of biomass. Extensive experiments have been recently performed by Di Blasi and his co-workers [2–6] to better understand the pyrolytic behaviour of loose-packed straw beds, products of some wood varieties and agricultural residues. However, the issue of unreliable kinetic constants remains unresolved for product yield predictions. Hence, this issue deserves further investigation before extensive computer simulation and/or development of more advanced pyrolysis models can be proposed. Work is still in progress to provide an extensive set of data that can be better interpreted and generalised by the use of mathematical models taking into account the complex effects of transport phenomena and chemical reactions.

* Corresponding author. Tel.: +61 2 9717 3817; fax: +61 2 9717 9263.
*E-mail address:* Guan.Yeoh@ansto.gov.au (G.H. Yeoh).

0017-9310/$ - see front matter © 2007 Elsevier Ltd. All rights reserved.
doi:10.1016/j.ijheatmasstransfer.2007.01.008

**Nomenclature**

| | |
|---|---|
| $a$ | mass fraction of virgin (unconverted) wood $\equiv (\rho_s - \rho_f)/(\rho_w - \rho_f)$ |
| $A_p$ | pre-exponential constant in Arrhenius equations |
| $C_p$ | specific heat capacity |
| $D$ | mass diffusivity |
| $E_p$ | activation energy in Arrhenius equations |
| $\sqrt{g}$ | Jacobian determinant |
| $h_c$ | heat transfer coefficient |
| $K_1$, $K_2$ | constants to Eq. (6) |
| $K_{D1}$, $K_{D2}$ | constants to Eq. (9) |
| $\dot{m}$ | mass flux |
| $M$ | molar mass |
| $n$ | normal direction to boundary surface |
| $P$ | pressure |
| $P_0$ | atmospheric pressure |
| $P_s$ | total pressure |
| $R_{ev}$ | rate of evaporation |
| $R_g$ | universal gas constant |
| $R_p$ | rate of pyrolysis |
| $t$ | time |
| $T$ | temperature |
| $x$, $y$, $z$ | Cartesian coordinates |
| $X_0$ | initial moisture content |

*Greek symbols*

| | |
|---|---|
| $\alpha_s$ | mass transfer coefficient of solid |
| $\beta_{ki}$, $\beta_{kj}$ | adjugate Jacobian metric element |
| $\Delta H_{ev}$ | heat of evaporation |
| $\Delta H_p$ | heat of pyrolysis |
| $\varepsilon$ | surface emissivity |
| $\lambda$ | thermal conductivity |
| $\mu$ | dynamic viscosity |
| $\nu$ | kinematic viscosity |
| $\pi_g$ | porosity of solid |
| $\theta_s$ | modified solid temperature |
| $\rho$ | density |
| $\rho_t$ | sum of densities |
| $\sigma$ | Stefan–Boltzmann constant |
| $\xi^l$ | $l$th non-orthogonal coordinate |

*Subscripts*

| | |
|---|---|
| a | active portion of pyrolysing solid |
| c | carbon |
| f | final char; furnace temperature |
| g | volatile gas; furnace gas temperature |
| i | inert |
| $j$ | Indices |
| l | liquid |
| ref | reference |
| s | solid |
| so | wood surface |
| v | vapour |
| vs | saturated vapour |
| w | virgin wood |

*Superscripts*

| | |
|---|---|
| $k$ | $\equiv x, y, z$ – directions along (parallel) and across (perpendicular) grains of wood |

An important area in the analysis of fires is the phenomena of flame spread over a combustible wall. Jia et al. [7] have successfully performed a three-dimensional (3-D) numerical study of the combustion of non-charring solid fuels – polymethylmethacrylate (PMMA) – in a small compartment. Nevertheless, we have recently applied a 3-D CFD-based fire model incorporating combustion and radiation with the additional consideration of a relatively simple wood pyrolysis sub-model within the fire model to simulate fire growth and flame spread over a vertical timber wall in an enclosure [8]. Model predictions have yielded good qualitative agreement with the transient development of the observed fire behaviour during experiments. In order that more effective predictions can be made with the fire model, the increase in sophistication of the wood pyrolysis model is required to comprehensively account for the anisotropic, hygroscopic and kinetic properties of wood.

Ever since the development of a one-dimensional (1-D) mathematical model for wood pyrolysis by Bamford et al. [9], experiments using wood samples of various sizes and shapes heated inside furnaces with closely controlled temperatures and non-oxidising environments have been performed to determinate the kinetic data for the validation of models. Transient quantities including the mass loss and temperature rise of the samples are usually measured. The 1-D mathematical models for the pyrolysis of dry wood have been employed to estimate the kinetic data of the wood pyrolysis by Tinney [10], Kanury and Blackshear [11], Kanury [12] and Kung and Kalelkar [13,14]. Roberts [15] reviewed the kinetic data and concluded that they were dependent on the size of the sample. Alves and Figueiredo [16] proposed further a 1-D model for the pyrolysis of wet wood with six-reaction schemes taking into account the different constituents in wood such as hemicellulose, cellulose and lignin, where the corresponding kinetic data were obtained by method of multistage isothermal thermogravimetry. Fredlund [17,18] and Di Blasi [19,20] proposed 2-D models with the consideration of pressure driven internal convection of gases in the pyrolysing wood. The former model considered moisture evaporation in wet wood pyrolysis, while the latter considered only dry wood pyrolysis with the primary and secondary reaction schemes following the work of Bradbury et al. [21] and Broido and Nelson [22]. The latter also recently applied the model to accommodate fast pyrolysis characteristics of cellulosic particles in fluid-bed reactors [23,24]. In this study, extra-particle

tar evolution has been described in addition to the primary char formation. Nevertheless, in the heating of a large cubical wood samples in furnaces, both 1-D and 2-D mathematical models for wood pyrolysis cannot precisely represent the boundary conditions. Bonnefoy et al. [25] have reported a 3-D model for wood pyrolysis and obtained the kinetic data for beech wood pyrolysis using the experimental mass loss measurements. Their model, however, has not considered the moisture content and the anisotropic nature of wood, nor the convective heat transfer as a result of the internal flows of volatile gases produced in the pyrolysis processes.

A 3-D mathematical model for the pyrolysis of wet wood is presented. The pyrolysis reaction is modelled by a first-order Arrhenius reaction, although six first-order reactions representing the competing thermal degradation reactions of various constituents such as the cellulose, hemicellulose, lignin and other minor constituents have been formulated. Evaporation of moisture inside the wood is handled through a consideration of the saturation vapour pressure. An energy equation incorporating heat conduction, internal convection due to movement of the water vapour, volatile and inert gases inside the pyrolysing wood as well as the heats of pyrolysis and evaporation has been formulated. The transport of gases and vapour through the charring solid is assumed to obey Darcy's Law. Mass conservation equations describing the vapour, volatile and inert gases in wood are considered. The anisotropic properties of wood including conductivities and permeabilities due to the structure of the grains in wood have been accounted for. The thermophysical properties of the charring wood has been assigned an extent-of-reaction and porosity dependence. The governing equations were transformed into a non-orthogonal curvilinear coordinate system, making the model applicable to a large range of arbitrary geometries. This model adequately captures the essential chemical processes where computational efficiency is maintained for practical simulations when it is solved in conjunction with the CFD-based fire model without substantially overburdening the computational resources through a more comprehensive model such as proposed by Di Blasi [23,24].

In this current analysis, the 3-D model had been used to predict the pyrolysis of a wooden cube inside a furnace under various temperatures. The transformed governing equations were solved numerically using a control volume technique. Simulations were performed for different initial moisture contents at furnace temperatures of 973 K and 1273 K. The activation energy and pre-exponential factor for the pyrolysis reaction of the single constituent have been adjusted to fit the measured mass loss history reported by Bonnefoy et al. [25]. Detailed results showing the transient development and distribution of the temperature, pressure, gases flow, moisture evaporation and char fraction for different furnace temperatures are presented. The effects of the grain structure and the presence of moisture on the heat and mass transfer in the pyrolysing wood are discussed.

## 2. Mathematical formulation

The 1-D mathematical models for wood pyrolysis have previously been applied for the determination of kinetic data for limited dimensions of slabs or cylindrical wood samples. However, for cubical wood samples, the pyrolysis, which involves the interactions between the chemical and physical processes in the solid, must be modelled by a 3D pyrolysis model incorporating the moisture content, anisotropic properties of wood and the internal convection of gases. The presence of moisture in hygroscopic materials such as wood will have a significant effect on their characteristics of ignition and hence affect their combustibility.

In the current model, the rate of pyrolysis is described by a first-order Arrhenius reaction

$$R_{\mathrm{p}} = -\frac{\partial \rho_{\mathrm{a}}}{\partial t} = \rho_{\mathrm{a}} A_{\mathrm{p}} \exp[-E_{\mathrm{p}}/(R_{\mathrm{g}} T_{\mathrm{s}})] \tag{1}$$

where $\rho_{\mathrm{a}}$ is the density of the active volatile portion of wood; $A_{\mathrm{p}}$ is the pre-exponential constant; $E_{\mathrm{p}}$ is the activation energy for the pyrolysis reaction; $R_{\mathrm{g}}$ is the universal gas constant; and $T_{\mathrm{s}}$ is the local solid temperature. Although a single first-order reaction has been used here, the pyrolysis model has been formulated to accommodate multiple reactions accounting for the competing reactions of up to six constituents in the solid.

The heat transfer in the solid occurs by thermal conduction and internal convection. The conservation equation for energy is expressed in a non-orthogonal curvilinear coordinate system $\xi^i$ by the following equation:

$$\begin{aligned}\sqrt{g}\frac{\partial[(\rho_{\mathrm{s}} C_{ps} + \rho_{\ell} C_{p\ell})\theta_{\mathrm{s}}]}{\partial t} = {} & \frac{\partial}{\partial \xi^i}\left(\beta_{ki}\beta_{kj}\lambda_{\mathrm{s}}^k \frac{\partial \theta_{\mathrm{s}}}{\partial \xi^j}\right) \\ & - \frac{\partial[\beta_{ki}(\dot{m}_{\mathrm{g}}^k C_{pg} + \dot{m}_{\mathrm{v}}^k C_{pv} + \dot{m}_{\mathrm{i}}^k C_{pi})\theta_{\mathrm{s}}]}{\partial \xi^i} \\ & - \sqrt{g}(\Delta H_{\mathrm{p}} R_{\mathrm{p}} + \Delta H_{\mathrm{ev}} R_{\mathrm{ev}})\end{aligned} \tag{2}$$

where $C_p$, $\Delta H_{\mathrm{p}}$ and $\Delta H_{\mathrm{ev}}$ are the specific heat capacities, heat of pyrolysis and evaporation, respectively, defined with reference to a datum $T_{\mathrm{ref}}$; $\theta_{\mathrm{s}} = T_{\mathrm{s}} - T_{\mathrm{ref}}$ is the modified solid temperature; $R_{\mathrm{ev}}$ is the rate of moisture evaporation. The superscript $k = x, y, z$ denotes the directions along (i.e. parallel) and across (i.e. perpendicular) grains to account for the anisotropic properties of wood. The mass fluxes and densities are denoted by $\dot{m}$ and $\rho$. The vapour and inert gases are assumed to be present initially in the wood at ambient conditions. Also, $\lambda_{\mathrm{s}}$ represents the thermal conductivity of the charring wood. $\beta_{ki}$, $\beta_{kj}$ and $\sqrt{g}$ represent the geometric coefficients and the Jacobian of the non-orthogonal curvilinear transformation.

The transfer of the vapour, volatile and inert gases is assumed to obey Darcy's Law, with the transfer coefficient $\alpha_{\mathrm{s}}^k$ given by the ratio of permeability $D_{\mathrm{s}}^k$ to kinematic viscosity $v_{\mathrm{s}}$ of the mixture. The total mass flux is

$$\dot{m}^k = -\frac{\alpha_s^k}{\sqrt{g}}\beta_{kj}\frac{\partial P_s}{\partial \xi^j} \tag{3}$$

where $\alpha_s^k = D_s^k/v_s$. The kinematic viscosity of the mixture is defined by $v_s = \mu_s/\rho_t$ where $\mu_s$ is the dynamic viscosity of the mixture; $\rho_t = \rho_g + \rho_i + \rho_v$ is the sum of the densities of vapour, volatile and inert gases; and $P_s$ is the total pressure given by the sum of the partial pressures of vapour, volatile and inert gases, $P_s = P_g + P_i + P_v$. The dynamic viscosity of the mixture is determined by the weighted sum of the dynamic viscosities of the gaseous species in wood. Individual mass fluxes of the vapour, volatile and inert gases are obtained by weighted fractions of the total mass flux with respect to the gaseous species densities.

The equations for the conservation of mass (i.e. continuity) of the vapour, volatile and inert gases expressed in non-orthogonal curvilinear coordinate system are given as

$$\frac{\partial \rho_v}{\partial t} = \frac{1}{\sqrt{g}}\frac{\partial}{\partial \xi^i}\left(\frac{\alpha_s^k \rho_v}{\rho_t}\beta_{ki}\beta_{kj}\frac{\partial P_s}{\partial \xi^j}\right) + R_{ev} \tag{4}$$

$$\frac{\partial \rho_g}{\partial t} = \frac{1}{\sqrt{g}}\frac{\partial}{\partial \xi^i}\left(\frac{\alpha_s^k \rho_g}{\rho_t}\beta_{ki}\beta_{kj}\frac{\partial P_s}{\partial \xi^j}\right) + R_p \tag{5}$$

$$\frac{\partial \rho_i}{\partial t} = \frac{1}{\sqrt{g}}\frac{\partial}{\partial \xi^i}\left(\frac{\alpha_s^k \rho_i}{\rho_t}\beta_{ki}\beta_{kj}\frac{\partial P_s}{\partial \xi^j}\right) \tag{6}$$

The vapour, volatile and inert gases are assumed to obey the ideal gas law. The densities of individual gases are assigned a dependence on porosity.

A combined pressure equation representing the conservation of mass is obtained through

$$\sqrt{g}\frac{\partial(\pi_g P_s/R_g T_s)}{\partial t} = \frac{\partial}{\partial \xi^i}\left[\frac{\alpha_s^k}{\rho_t}\left(\frac{\rho_v}{M_\ell} + \frac{\rho_g}{M_g} + \frac{\rho_i}{M_i}\right)\beta_{ki}\beta_{kj}\frac{\partial P_s}{\partial \xi^j}\right] + \sqrt{g}\left(\frac{R_{ev}}{M_\ell} + \frac{R_p}{M_g}\right) \tag{7}$$

where $M$ is the molar mass and $\pi_g$ is the porosity.

The evaporation of moisture in the wood is assumed to be sufficiently rapid to attain thermodynamic equilibrium, i.e. $P_v = P_{vs}$, with the saturation vapour pressure $P_{vs}$ given by

$$P_{vs} = K_1 \exp(-K_2/T_s) \tag{8}$$

where $K_1$ and $K_2$ are constants relevant to the temperature range being studied. The rate of evaporation of moisture is given by

$$R_{ev} = \frac{\partial \rho_v}{\partial t} - \frac{1}{\sqrt{g}}\frac{\partial}{\partial \xi^i}\left(\frac{\alpha_s^k \rho_v}{\rho_t}\beta_{ki}\beta_{kj}\frac{\partial P_s}{\partial \xi^j}\right) \tag{9}$$

The thermal conductivity $\lambda_s^k$ and volumetric heat capacity $\rho_s C_{ps}$ of the pyrolysing wood are normally assumed to vary linearly with char fraction from the initial value of the virgin wood to that of the char [17,19,20]

$$\lambda_s^k = a\lambda_w^k + (1-a)\lambda_f^k;$$
$$\rho_s C_{ps} = a\rho_w C_{pw} + (1-a)\rho_f C_{pf} \tag{10}$$

where $\lambda_w^k$, $\lambda_f^k$, $C_{pw}$ and $C_{pf}$ are the thermal conductivities and specific heat capacities of the virgin wood and final char respectively and $a = (\rho_s - \rho_f)/(\rho_w - \rho_f)$. The final char density ($\rho_f$) is assumed to be known *a priori*.

The permeability of the pyrolysing solid is described by an exponential function of the varying solid density as the wood progressively transforms to char:

$$D_s^k = K_{D1}^k \exp(-K_{D2}^k c) \tag{11}$$

where $c$ is a function of char fraction. The variables $K_{D1}^k$ and $K_{D2}^k$ are constants depending on species and orientation of the wood grains. All other thermodynamic and transport properties are taken to vary linearly with temperature. Thermal swelling, shrinkage, surface regression and possible surface oxidation reactions of the virgin wood and char are neglected.

## 3. Numerical details

The conservation equations were discretised using a control volume technique. A hybrid differencing scheme was employed for the convection term. The discretised equations were solved using the Stone's Strongly Implicit Procedure [26]. The 3-D pyrolysis model has been used to simulate pyrolysis of a wooden cube of dimensions 10 mm × 10 mm × 10 mm. Taking advantage of the cubical shape, only one-eighth of the cube was considered as the domain for simulation. Fig. 1a shows the computational domain with reference to the actual dimension of the cube. A total of 15 × 15 × 15 control volumes in the directions along and across the grains were used. A non-uniform mesh was used in the wood with the mesh concentrated adjacent to the heated external surfaces of the cube, to account for the steep gradients (see Fig. 1b).

### 3.1. Boundary conditions

The cubical wood is heated by surrounding convection and radiation. The boundary conditions for the governing energy and pressure equations at the planes of symmetries at $x = 5$ mm, $y = 5$ mm and $z = 5$ mm are

$$\frac{\partial T_s}{\partial n} = 0 \quad \text{and} \quad \frac{\partial P_s}{\partial n} = 0 \tag{12}$$

and those for the heated external surfaces at $x = 0$, $y = 0$ and $z = 0$ are

$$\lambda_s^n \frac{\partial T_s}{\partial n} = -\varepsilon\sigma(T_{s0}^4 - T_f^4) - h_c(T_{s0} - T_g); \quad P_s = P_0 \tag{13}$$

where $\varepsilon$ denotes the surface emissivity; $\sigma$ is the Stefan–Boltzmann constant; $T_{s0}$ the wood surface temperature; $T_f$ the furnace temperature; $T_g$ the furnace gas temperature; the ambient pressure $P_0$ is taken to be at 1.013 bar and $n$ denotes the direction normal to the boundary surface.

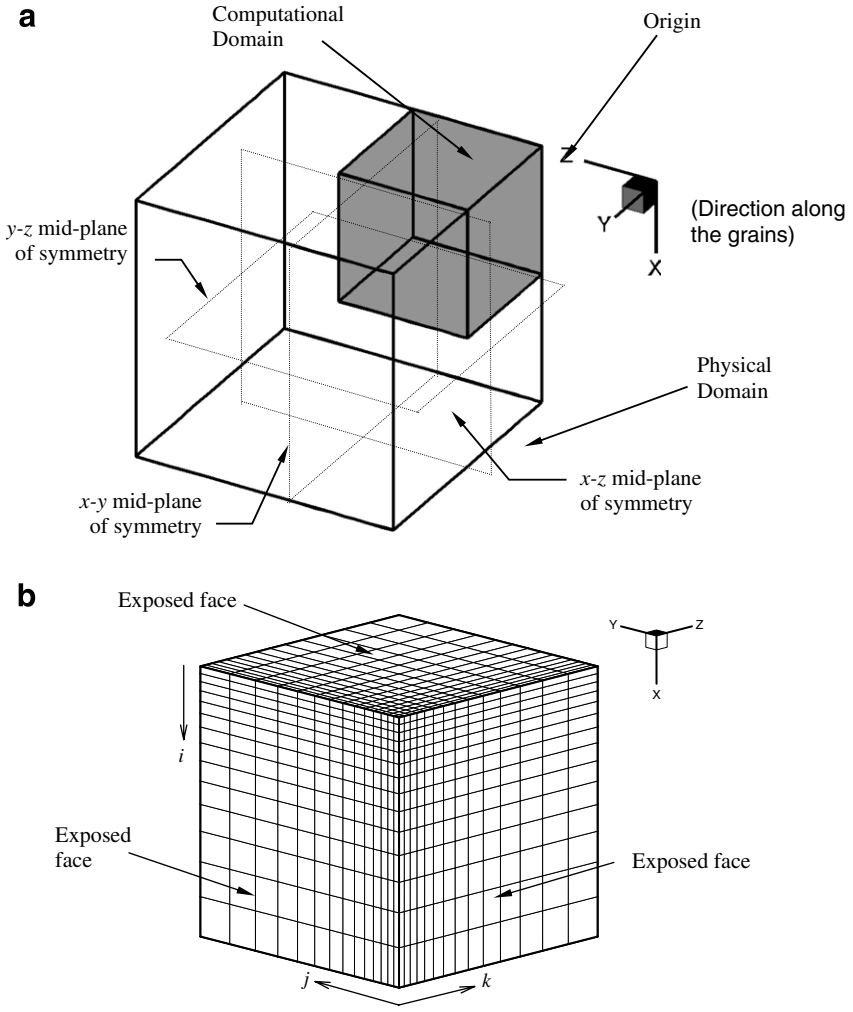


Fig. 1. Pyrolysis of a wooden cube: (a) physical and computational domain of the wooden cube (the wood grains are parallel to the $x$-axis) and (b) mesh distribution.

### 3.2. Property values

Computations have been performed using the current 3-D pyrolysis model for wooden cubes of 0% and 9% initial moisture contents at the furnace temperatures of 973 K and 1273 K. The initial temperatures of the wood and ambient were assumed to be 25 °C. The emissivity of the surface of the wood was assumed to be 0.85.

The constants $K_1$ and $K_2$ for expression of the saturated vapour pressure are $4.143 \times 10^4$ MPa and 4822 K respectively for the range of temperatures studied. The specific heats were taken to be

$$C_{pw} = 1400 + 0.3\theta_s \text{ J kg}^{-1} \text{ K}^{-1} \quad (14)$$

$$C_{pf} = 700 + 0.6\theta_s \text{ J kg}^{-1} \text{ K}^{-1} \quad (15)$$

$$C_{p\ell} = 4190 \text{ J kg}^{-1} \text{ K}^{-1} \quad (16)$$

$$C_{pg} = 1000 + 0.8\theta_s \text{ J kg}^{-1} \text{ K}^{-1} \quad (17)$$

$$C_{pi} = 1062.9 \text{ J kg}^{-1} \text{ K}^{-1} \quad (18)$$

$$C_{pv} = 1880 \text{ J kg}^{-1} \text{ K}^{-1} \quad (19)$$

For anisotropic properties of wood, the thermal conductivities and permeabilities of the virgin wood and char are given by [17,19,20]

$$\lambda_w^x = 0.255 \text{ W m}^{-1} \text{ K}^{-1} \quad (20)$$

$$\lambda_f^x = 0.1046 \text{ W m}^{-1} \text{ K}^{-1} \quad (21)$$

$$\lambda_w^y = \lambda_w^z = 0.105 \text{ W m}^{-1} \text{ K}^{-1} \quad (22)$$

$$\lambda_f^y = \lambda_f^z = 0.071 \text{ W m}^{-1} \text{ K}^{-1} \quad (23)$$

and

$$K_{D1}^x = 4.935 \times 10^{-14} \text{ m}^2 \quad (24)$$

$$K_{D2}^x = 4.605 \quad (25)$$

$$K_{D1}^y = K_{D1}^z = 4.935 \times 10^{-18} \text{ m}^2 \quad (26)$$

$$K_{D2}^y = K_{D2}^z = 11.513 \quad (27)$$

The dynamic viscosities for the gas species in wood were taken to be

$$\mu_g = 8.5 \times 10^{-6} + 0.0295 \times 10^{-6}\theta_s \text{ kg m}^{-1}\text{ s}^{-1} \quad (28)$$

$$\mu_v = 8.5 \times 10^{-6} + 0.0375 \times 10^{-6}\theta_s \text{ kg m}^{-1}\text{ s}^{-1} \quad (29)$$

$$\mu_i = 3.178 \times 10^{-5} \text{ kg m}^{-1}\text{ s}^{-1} \quad (30)$$

The molecular weights for the various gas species in both the solid and gas phase were assumed to be: $M_g = 75$, $M_v = 18$ and $M_i = 28$. The heat of pyrolysis $\Delta H_p = 322 \text{ kJ kg}^{-1}$ (endothermic) has been adopted. The heat of evaporation $\Delta H_{ev}$ was taken to be $2260 \text{ kJ kg}^{-1}$. The final char density $\rho_f$ and the initial wood density, $\rho_w$ of $91.56 \text{ kg m}^{-3}$ and $700 \text{ kg m}^{-3}$, were respectively used.

## 4. Mass loss experiment

Fig. 2 presents the experimental setup by Bonnefoy et al. [25] for the determination of mass loss of pyrolysing wooden cubes in a furnace. The electrical furnace with a cylindrical quartz reactor was used to provide heating to the wood sample at a precisely controlled furnace temperature. The quartz reactor heated in the furnace was moved rapidly to bring the wood cube to the centre of the furnace, which was an isothermal zone. During the experiments, wood samples were placed in a platinum wire cell attached to an electronic balance to continuously monitor mass loss. The balance was connected to a microcomputer for data acquisition. A stream of nitrogen gas at a controlled flowrate of $200 \text{ l h}^{-1}$ was maintained in the experiments. Thermocouples were placed along the axis of the reactor. The wood surface temperature was also recorded by a thermocouple placed under the wood cube. However, during pyrolysis, the thermocouples were found to penetrate inside the wood and the surface temperatures resulting from the experiments were found not to represent the true surface temperature.

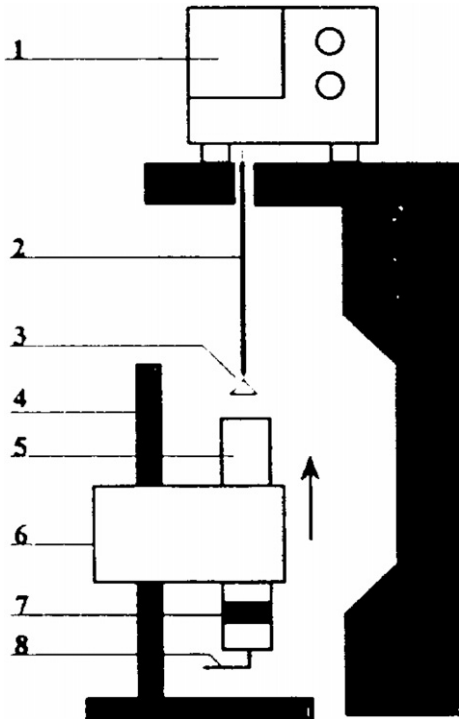


Fig. 2. Experimental setup: (1) balance; (2) alumina coating; (3) platinum cell + thermocouple; (4) mobile support of furnace; (5) quartz reactor; (6) furnace; (7) honeycomb and (8) gas inlet (extracted from paper by Bonnefoy et al. [25]).

## 5. Results and discussion

### 5.1. Mass fraction loss

A wide range of values of kinetic data i.e. the activation energy $E_p$ and the pre-exponential factor $A_p$ has been reported. Typical values can be found in [9–15]. However, these values have been obtained by fitting experimentally determined mass loss due to pyrolysis of wood using 1-D models for dry wood. Only the 1-D model by Alves and Figueiredo [16] incorporated moisture vaporisation in wood during pyrolysis. All these models are still limited to 1-D applications. To determine these values for the current 3-D model, simulations of the pyrolysis of a wet wooden cube with an initial moisture content $X_0 = 9\%$ at furnace temperatures $T_f = 973$ K and $T_f = 1273$ K were performed. The computed mass loss histories were compared with the experimental results on beech wood by Bonnefoy et al. [25]. Fig. 3 shows the best agreement achieved between the computed and experimental mass

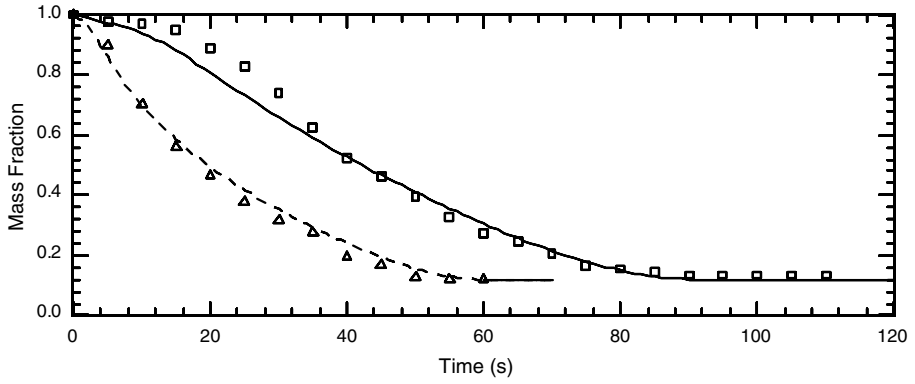


Fig. 3. The computed transient mass fraction loss at the furnace temperature of 973 K (—) and 1273 K (--), compared with experimental values at 973 K (□) and 1273 K (△) reported in [16].

losses against time for the pyrolysis of the wooden cube obtained using an activation energy $E_p = 125$ kJ mole$^{-1}$ and a pre-exponential factor $A_p = 1.25 \times 10^8$ s$^{-1}$. Excellent agreement is observed in the case of $T_f = 1273$ K. For $T_f = 973$ K, the computed and measured values agree extremely well after about 35 s until completion of pyrolysis (i.e. during the middle and final stages). In the early stage, however, discrepancy arises probably due to the use of only a single kinetic reaction for the modelling of the devolatilisation process. It is well known that competing primary reactions due to the different major constituents (i.e. cellulose, hemicellulose and lignin) and secondary reactions exist in wood pyrolysis [19]. Since the current computational code has been formulated with multiple competing reactions for the major constituents, the prediction may be improved if these reactions

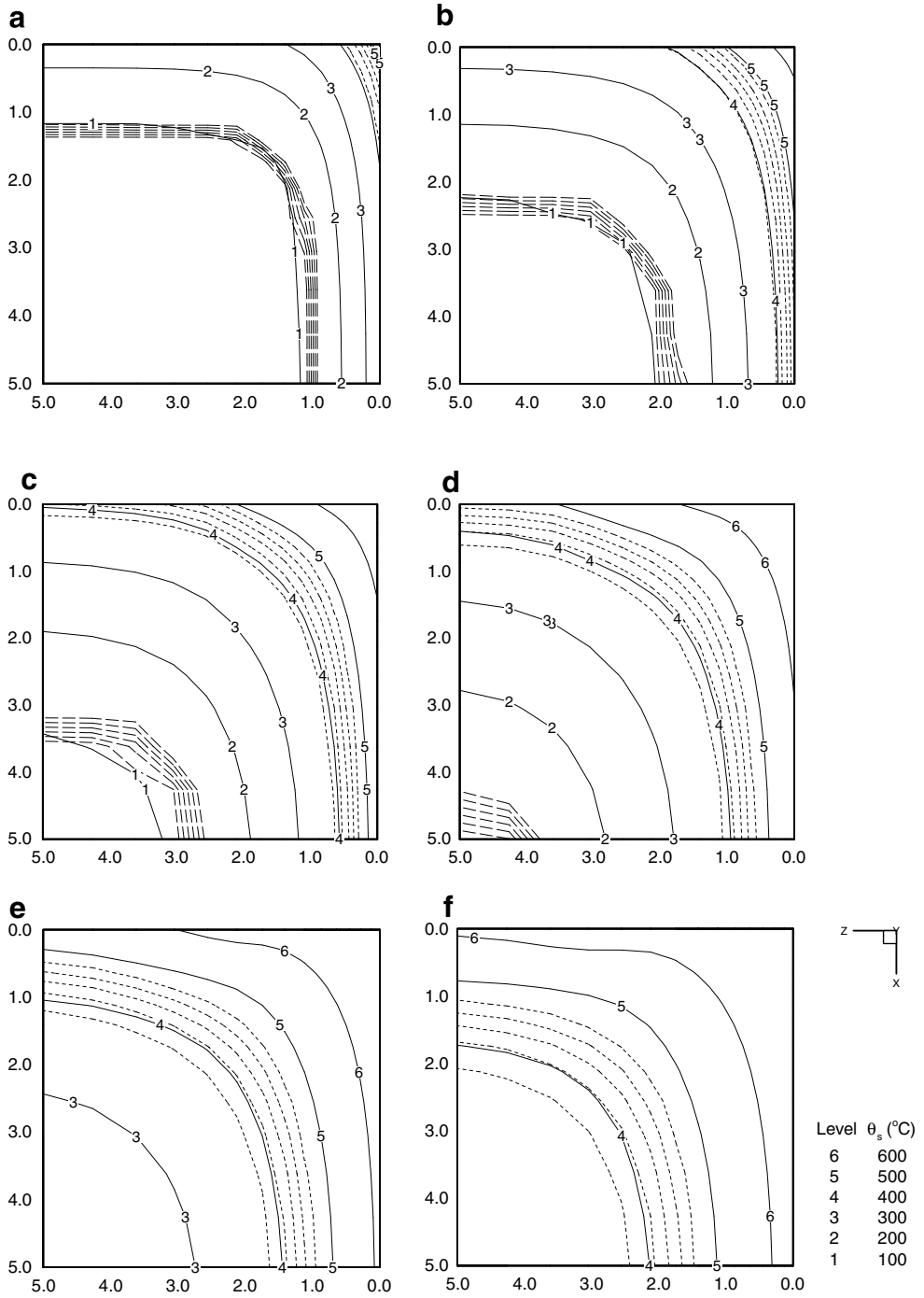


Fig. 4. Distribution of isotherms (—) from 100 °C to 600 °C, char fraction contours (---) from 0.02 to 0.1 with step 0.02 and moisture content contours (––) from 2% to 7% with step 1% on $y$–$z$ plane at $x = 5$ mm (mid-plane) for $T_f = 973$ K and $X_0 = 9\%$ at times: (a) 10 s, (b) 20 s, (c) 30 s, (d) 40 s, (e) 50 s and (f) 60 s.

are modelled. Nevertheless, the overall agreement is still considered to be very good. The selected values of activation energy and pre-exponential factor are also in good agreement with the values of $E_p = 124.7$ kJ mole$^{-1}$ and $A_p = 6 \times 10^7$–$7.5 \times 10^8$ s$^{-1}$ reported in [9]. The pre-exponential factor, however, is higher than the value of $5 \times 10^6$ s$^{-1}$ reported by Bonnefoy et al. [25]. This is probably due to the absence of the moisture evaporation in their 3-D model. As the presence of the evaporation processes appears to slow down the initial process of temperature rise in wood, a higher value of pre-exponential factor is expected in the current model, which includes the consideration of moisture evaporation.

### 5.2. Transient contours

Computed transient results for the wet wood of $X_0 = 9\%$ heated at a furnace temperature of 973 K and 1273 K are presented and discussed below.

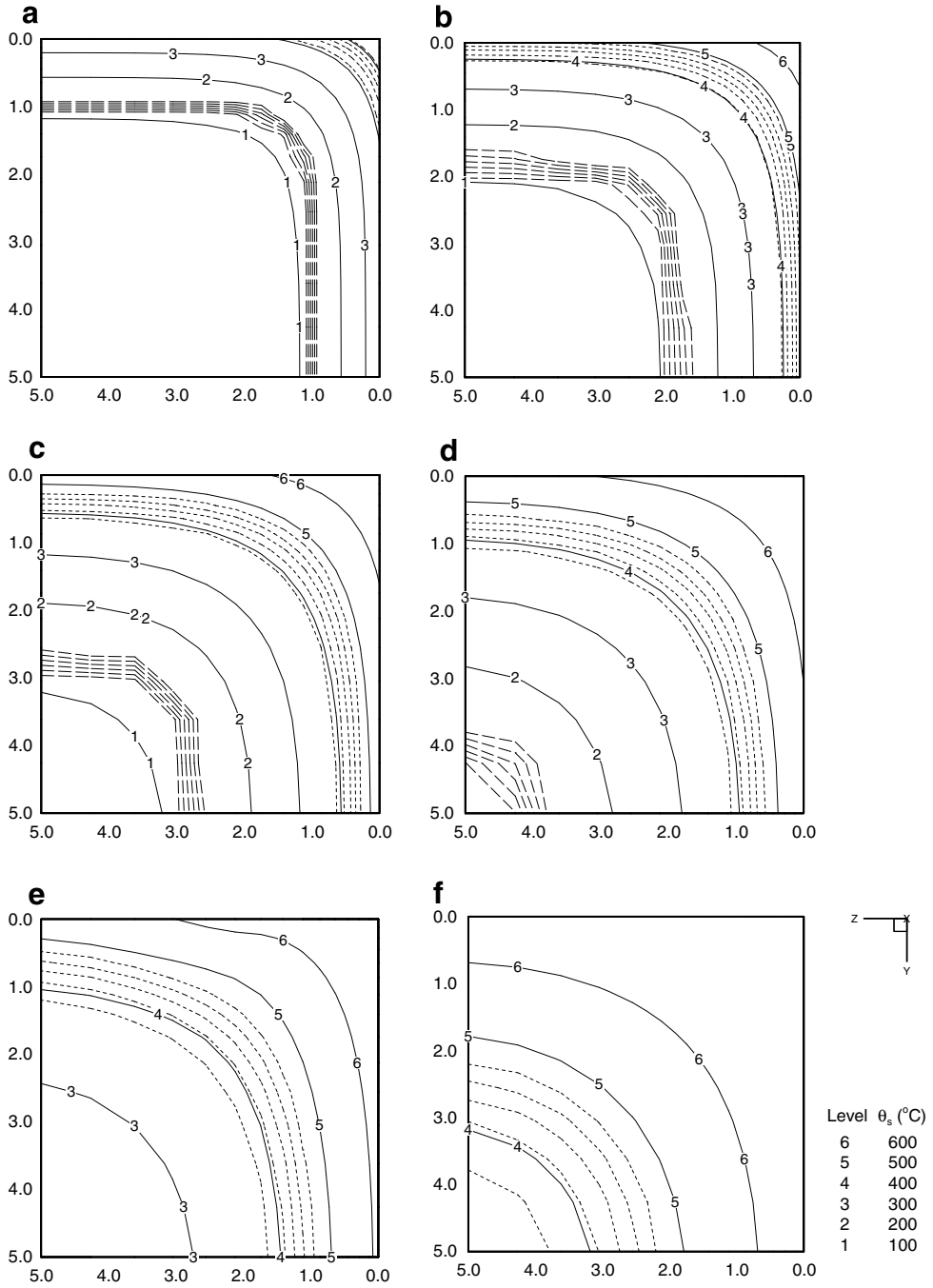


Fig. 5. Distribution of isotherms (—) from 100 °C to 600 °C, char fraction contours (---) from 0.02 to 0.1 with step 0.02 and moisture content contours (–·–) from 2% to 7% with step 1% on $x$–$z$ plane at $y = 5$ mm (mid-plane) for $T_f = 973$ K and $X_0 = 9\%$ at times: (a) 10 s, (b) 20 s, (c) 30 s, (d) 40 s, (e) 50 s and (f) 60 s.

*5.2.1. Isotherms and char fraction and moisture content contours*

Fig. 4 shows the isotherms together with the char fraction ($\rho_c/\rho_w$) and moisture content contours in the cube from $t = 10$–60 s for the furnace temperature of 973 K, on the $x$–$z$ plane at $y = 5$ mm (mid-plane) cutting parallel to the direction of grains. A wave-like propagation exists for the isotherms from the external surfaces towards the centre of the cube as heating is applied. The temperature gradients are found to be generally smaller in the $x$-direction (along the grains) than in the $z$-direction (across the grains) due to the relatively higher thermal conductivities in the former direction. However, the rate of advancement of the isotherms is slower in the direction along the grains. This is due to the presence of large convective cooling as a result of internal flow of vapour and volatile gases in this direction, as reported previously by Di Blasi [19,20]. It is also revealed that the evaporative cooling due to the quicker and earlier evaporation of moisture along the grains serves to enhance this phenomenon. The contours

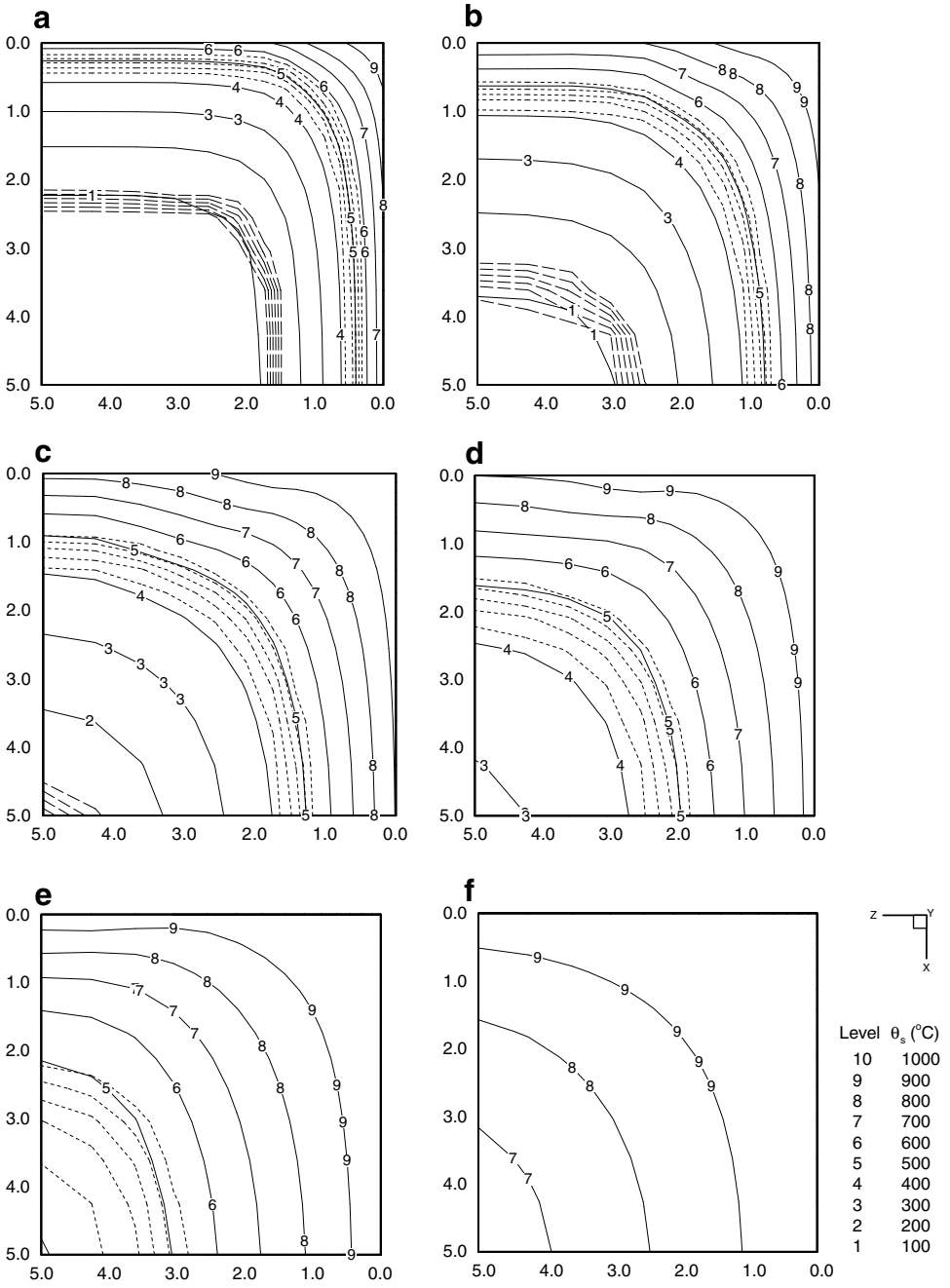


Fig. 6. Distribution of isotherms (—) from 100 °C to 600 °C, char fraction contours (---) from 0.02 to 0.1 with step 0.02 and moisture content contours (–·–) from 2% to 7% with step 1% on $y$–$z$ plane at $x = 5$ mm (mid-plane) for $T_f = 1273$ K and $X_0 = 9\%$ at times: (a) 10 s, (b) 20 s, (c) 30 s, (d) 40 s, (e) 50 s and (f) 60 s.

of moisture content indicate an advancing zone of evaporation. The innermost contour represents a content of 7% while the outermost is at 1%. Similar to the isotherms, a wave-like propagation also persists with the moisture content contours. The evaporation zone clearly separates the wet region (the absence of evaporation) from the dry region (the completion of evaporation). As expected, the evaporation occurs generally around a temperature of 100 °C. It is interesting to note that in the $x$-direction along the grains, the contour of 7% moisture content, which represents the onset of evaporation (i.e. evaporation front), always moves ahead of the 100 °C isotherm. In the $z$-direction across the grains, however, the evaporation front always falls behind the 100 °C isotherm. This implies that in direction along the grains, the evaporation begins at temperature slightly lower than 100 °C, while in the direction across the grains, it begins at slightly above 100 °C. This earlier process of the evaporation of moisture can be explained by the higher permeability in the direction along the grains, which allows the rapid release of vapour. A faster evaporation rate is

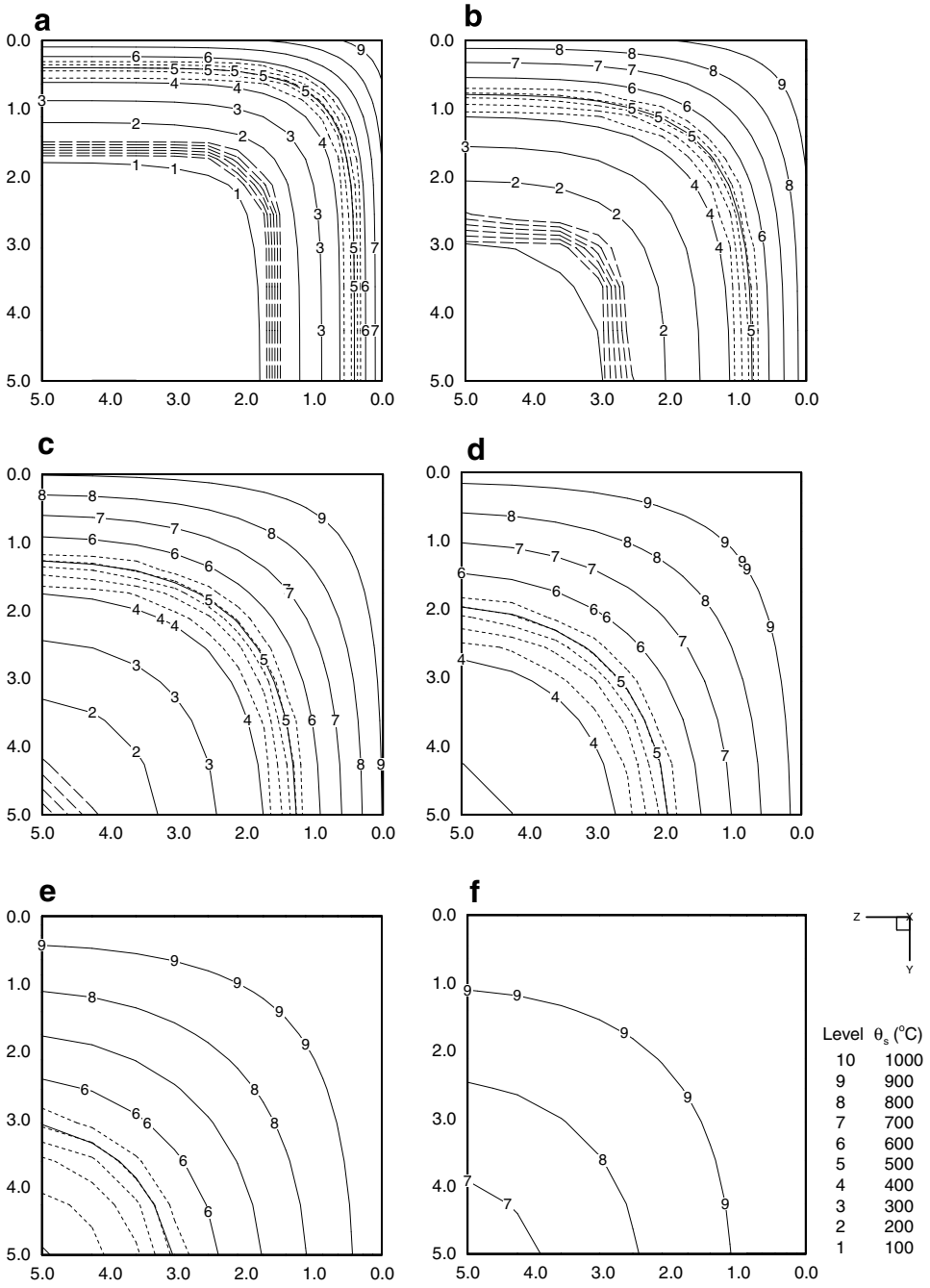


Fig. 7. Distribution of isotherms (—) from 100 °C to 600 °C, char fraction contours (---) from 0.02 to 0.1 with step 0.02 and moisture content contours (––) from 2% to 7% with step 1% on $x$–$z$ plane at $y = 5$ mm (mid-plane) for $T_f = 1273$ K and $X_0 = 9\%$ at times: (a) 10 s, (b) 20 s, (c) 30 s, (d) 40 s, (e) 50 s and (f) 60 s.

required to provide sufficient vapour to maintain saturation inside the porous medium and it appears that this assists in cooling the pyrolysing solid. It can therefore be inferred that the rate of evaporation of moisture in wood is affected by its permeability and by the grain structure. At 40 s, the evaporation zone approaches the centre of the cube leaving behind a large region of dry wood. Beyond 50 s, simulations predicted that the wood is completely dry. Fig. 4 also shows the contours of char fraction from 0.02 (≈15% char) to 0.10 (≈ 85% char). The region bounded by the char fraction contours of 0.02 and 0.1 represents the zone of active devolatilisation in the dry wood region. Similar to the isotherms, the wave-like behaviour is again prevalent with the char fraction contour of 0.02 representing the char front, which marches gradually towards the centre of the cube. The char fraction contour of 0.02 is found to march quicker in the $z$-direction (from right to left in the figures) towards the centre of the cube than that in the $x$-direction (from top to bottom). It follows very closely to the movement of isotherms of 400 °C and 500 °C throughout the heating process. Also, the region of devolatilisation stretches in time, as the temperature gradient becomes lower. At 80 s, the devolatilisation zone reaches the centre of the cube and the pyrolysis is completed at 90 s.

Fig. 5 illustrates the transient isotherms, char fraction and moisture content contours in the cube for the same furnace temperature as above, but on the $y$–$z$ plane at $x = 5$ mm (mid-plane) and perpendicular to the direction of the grains. The temperature gradients as indicated by the isotherms are identical along the $y$-axis and $z$-axis on the plane. This is expected due to the similar thermal conductivity and permeability in both directions which are perpendicular (i.e. across) to the grains. The rate of advancement of the isotherms is found to be the same for both transverse directions. The evaporation zone in the $x$–$z$ plane is bounded by the innermost (7%) and outermost (1%) contours has the similar wave-like propagation. Owing to the symmetrical nature of the boundary conditions and the thermophysical properties in the $y$-direction and $z$-direction, the rates of advancement of the evaporating zone towards the centre of the wooden cube are the same for both transverse directions. Nevertheless, due to the poor permeability of wood in the transverse directions, the vapour, once generated, is trapped inside the wood. This leads to the accumulation of vapour and hence the build-up of pressure above the atmospheric pressure inside the porous structure of the wood. Evaporation occurs above atmospheric pressure at around temperatures slightly above 100 °C. The phenomenon of this build-up

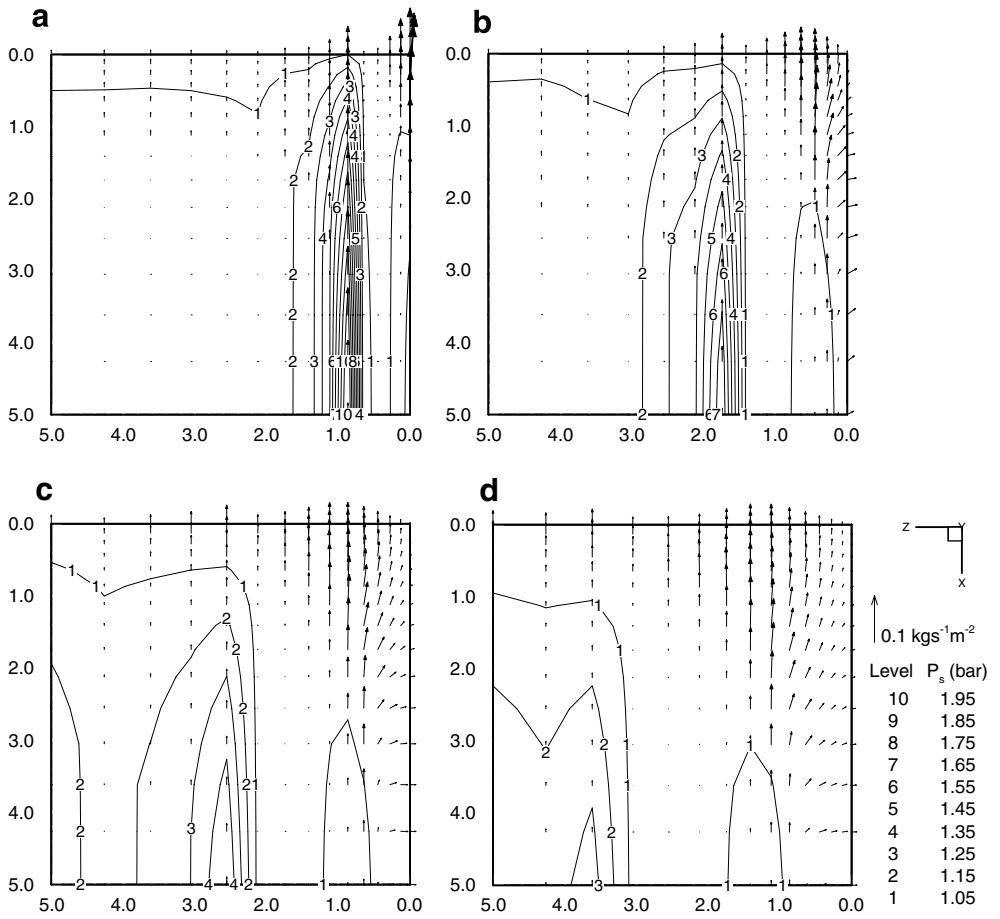


Fig. 8. Contours of total gas pressure and total mass flux vector field on $x$–$z$ plane at $y = 5$ mm (mid-plane) at times: (a) 10 s, (b) 20 s, (c) 30 s and (d) 40 s for $T_f = 973$ K and $X_0 = 9\%$.

of pressure can be confirmed with the isobars results, which will be discussed later in Fig. 8. As mentioned above and also seen here, the evaporation zone reaches the centre of the cube at 40 s leaving behind a large region of dry wood. The wood is completely dry after 50 s. Fig. 5 also shows that contours of char fraction from 0.02 to 0.10, indicating a region of active devolatilisation in the dry wood region, has the similar wave-like propagation behaviour. Since the devolatilisation process is temperature dependent according to the Arrhenius expression, the devolatilisation zone follows closely the advancement of the isotherms of 400 °C and 500 °C.

Figs. 6 and 7 present the isotherms, char fraction and moisture content contours in the cube from $t = 10$–60 s for the furnace temperature of 1273 K, on the $x$–$z$ plane at $y = 5$ mm (mid-plane) and on the $y$–$z$ plane at $x = 5$ mm (mid-plane) respectively. Owing to the higher furnace temperature, the isotherms march more rapidly in the $x$-direction along the grains than in the $z$-direction across the grains. As expected, quicker evaporation and devolatilisation of the cube exists at this higher temperature than that observed at the furnace temperature of 973 K. This is probably due to the larger convective cooling effects resulted from the internal flow of vapour and volatile gases in the $x$-direction along the grains. This applies equally also for the moisture content contours indicating the evaporation zone moving towards the centre of the cube at differential rates in $x$- and $z$-directions with similar trends for the char fraction contours. However, due to the higher furnace temperature and more rapid heating, the isotherms advance quicker towards the centre of the cube. In Figs. 6 and 7, the evaporation zone reaches the centre of the cube at 30 s. The wood is completely dry after 40 s. At 50 s, the devolatilisation zone arrives at the centre of the cube. The pyrolysis process is completed at 60 s.

### 5.2.2. Isobars and mass flux vector field

Fig. 8 consists of the isobars (total gas pressure contours) and total mass flux vector field from $t = 10$–40 s for the furnace temperature of 973 K, on the $x$–$z$ plane at $y = 5$ mm (mid-plane). The anisotropic effect of the wood undergoing pyrolysis can be best demonstrated through the transient flows and pressure contours. Here, a complex system of pressure and gas flows is observed. Three regions are identified. At $t = 10$ s, the region near to the left lower corner corresponds to the virgin wet wood that is neither evaporating nor pyrolysing. This zone consists of primarily

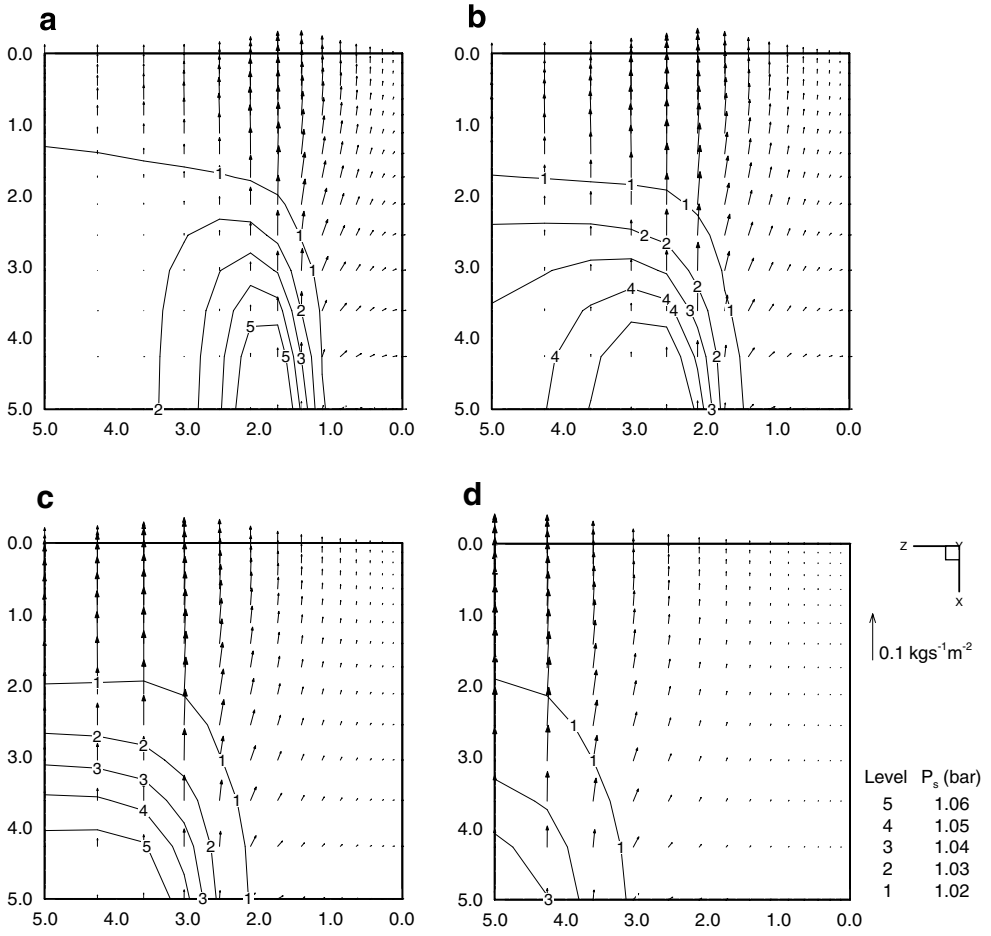


Fig. 9. Contours of total gas pressure and total mass flux vector field on $x$–$z$ plane at $y = 5$ mm (mid-plane) at times: (a) 50 s, (b) 60 s, (c) 70 s and (d) 80 s for $T_f = 973$ K and $X_0 = 9\%$.

saturated vapour and inert gases, which exists initially in the wood. In this zone, the pressure is below 1.05 bar but marginally higher than atmospheric pressure and is rising. This is because of the slow but gradually increasing temperature as well as the poor permeability of the virgin wood. Adjacent to this, a narrow region of high pressure is present. The elongated shape of the region with a steep pressure gradient across the grains is due to the much lower permeabilities of wood (i.e. 10,000 times less) in this direction than that along the grains. The highest value of the computed pressure is around 2.2 bar, which is in the same order of magnitude as the experimental value of 2.35 bar reported in [17]. This represents a region of rapid evaporation of the moisture in the wood. A third region of high pressure, around 1.15 bar – close to the right hand surface ($z = 0$) – corresponds to the onset of the devolatilisation after the drying of the wood. Pressure rise within the wood is due to the volatile gas being produced while the permeability remains low. The order of magnitude of the pressure in this region is comparable to the experimental value of 1.14 bar for the pyrolysis of dry wood [17]. As heating continues, evaporation begins in the inner part, which results in the migration of the high-pressure zone towards the centre of the cube. The devolatilisation zone is also found to move inwards following the evaporation zone. There is a tendency for a decrease of the peak pressure and pressure gradients in these two zones as the charred area expands near the top ($x = 0$) and right hand surfaces ($z = 0$) over time.

Total mass flux vectors indicating the magnitude and directions of flows of gases and vapour are illustrated in the same figure. The flow of gases and vapour are strongly governed by the grain structure with significant movement along the grains except near the surface $z = 0$. At the early stage around 20 s, while the devolatilisation is still concentrated at the right hand surface ($z = 0$), a considerable outflow of gases is evident at that surface. As the char front advances further into the wood and the charred area expands, the outflow of gases at the right hand surface becomes less significant. Two streams of gases leaving the top surface ($x = 0$) in Fig. 8 represent the outflow of the gases produced by the evaporation and devolatilisation. The stream above the pressure zone due to devolatilisation as discussed above consists mainly of volatile gases. The other stream, which follows closely the movement of the pressure zone due to evaporation, corresponds mainly to the outflow of vapour. At around 40 s, it disappears and the evaporation is completed.

Fig. 9 shows the total gas pressure contours and the total mass flux vector field in the cube from $t = 50$–$90$ s

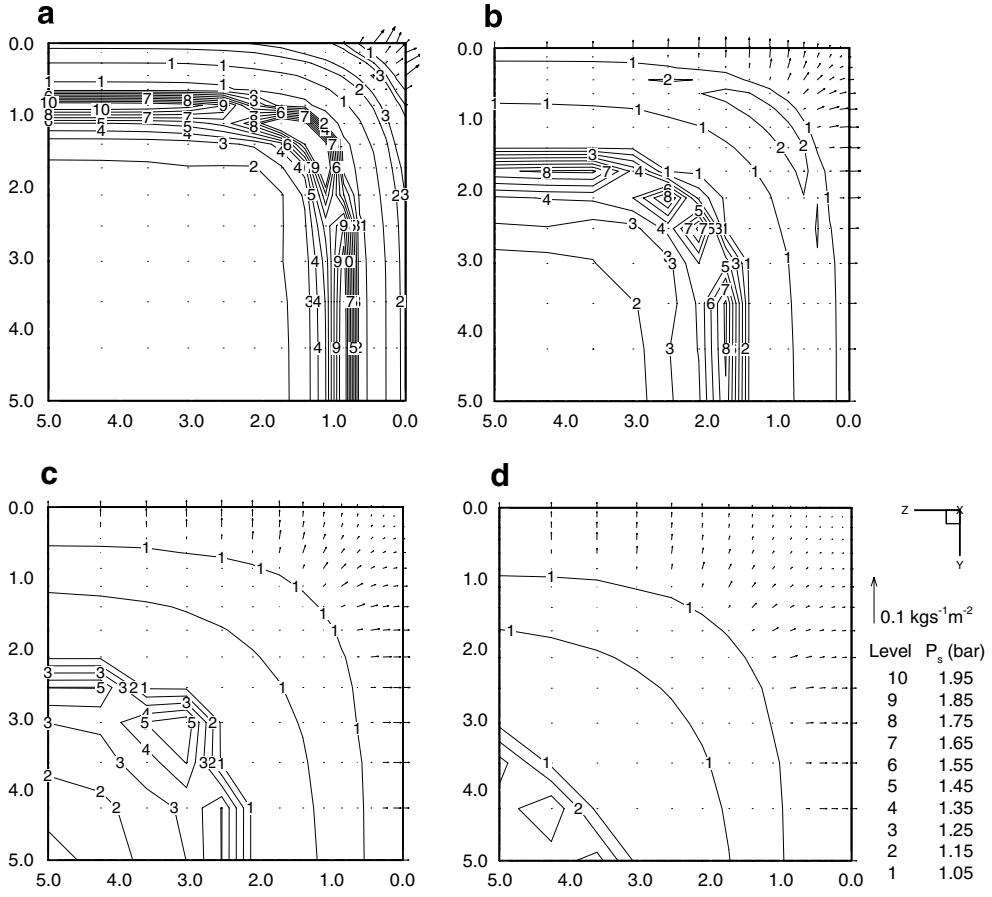


Fig. 10. Contours of total gas pressure and total mass flux vector field on $y$–$z$ plane at $x = 5$ mm (mid-plane) at times: (a) 10 s, (b) 20 s, (c) 30 s and (d) 40 s for $T_f = 973$ K and $X_0 = 9\%$.

for the same furnace temperature as above, but on the $x$–$z$ plane at $y = 0$ mm (mid-plane). Unlike the plots in Fig. 8, due to the completion of the evaporation in wood, only one zone with moderately high pressure is observed. This corresponds to the build-up of pressure because of the production of the volatile gases. Steeper pressure gradients are found in directions across the grains indicating again the effects of the structure of grain in wood on the internal flow of the gases in wood. Following the advancement of the isotherms towards the centre, the pressure region moves gradually towards the mid-plane ($z = 5$ mm). As shown by the mass flux vectors, the gas migrates and leaves the wood cube at the top surface ($x = 0$ mm) due to the grain orientation. With the formation of a large area of char near the top surface, there is an increase of outflow of gases from the top surface. The position of the maximum outflow follows closely the lateral movement of the high-pressure region and eventually reaches the mid-plane ($z = 5$ mm).

Fig. 10 illustrates the isobars and the total mass flux vector field from $t = 10$–40 s for the furnace temperature of 973 K, on the $y$–$z$ plane at $x = 5$ mm (mid-plane) cutting perpendicular to the direction of grains. Owing to the equal permeabilities and conductivities in the $y$-direction and $z$-direction (i.e. across the grains) and boundary conditions, the isobars and mass flux vector fields are symmetrical about the diagonal line from the origin of the computational domain. Here again, three regions are observed. The region near to the left lower corner, where the pressure is below 1.05 bar, corresponds to the region of virgin wet wood. Following this, a narrow strip formed by closely packed isobars is found, which corresponds to the zone where the temperature is around 100–150 °C where rapid evaporation of moisture content is occurring inside the wood cube. The vapour generated appears to be trapped because of the low permeabilities of wood. The peak pressure at this narrow high-pressure zone is above 1.95 bar. The third region of high pressure, around 1.25 bar, is found very close to the top right hand corner of the cube (i.e. $y = 0$ mm and $z = 0$ mm). This corresponds to zone where devolatilisation is occurring. From these results, two high-pressure zones corresponding to the evaporation of moisture and devolatilisation respectively propagate towards the centre of the cube like two consecutive waves (i.e. the devolatilisation zone moves inwards following the evaporation zone). In Fig. 10d, at $t = 40$ s, the high-pressure zone

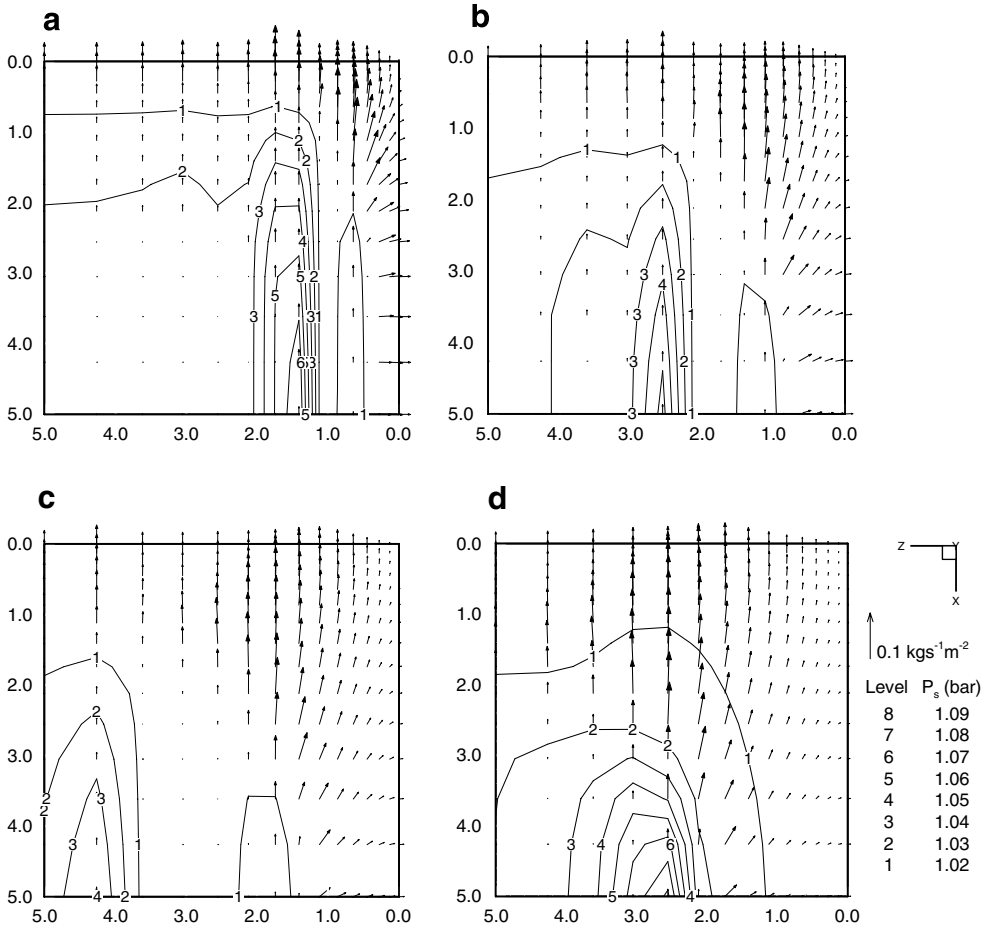


Fig. 11. Contours of total gas pressure and total mass flux vector field on $x$–$z$ plane at $y = 5$ mm (mid-plane) at times: (a) 10 s, (b) 20 s, (c) 30 s and (d) 40 s for $T_f = 1273$ K and $X_0 = 9\%$.

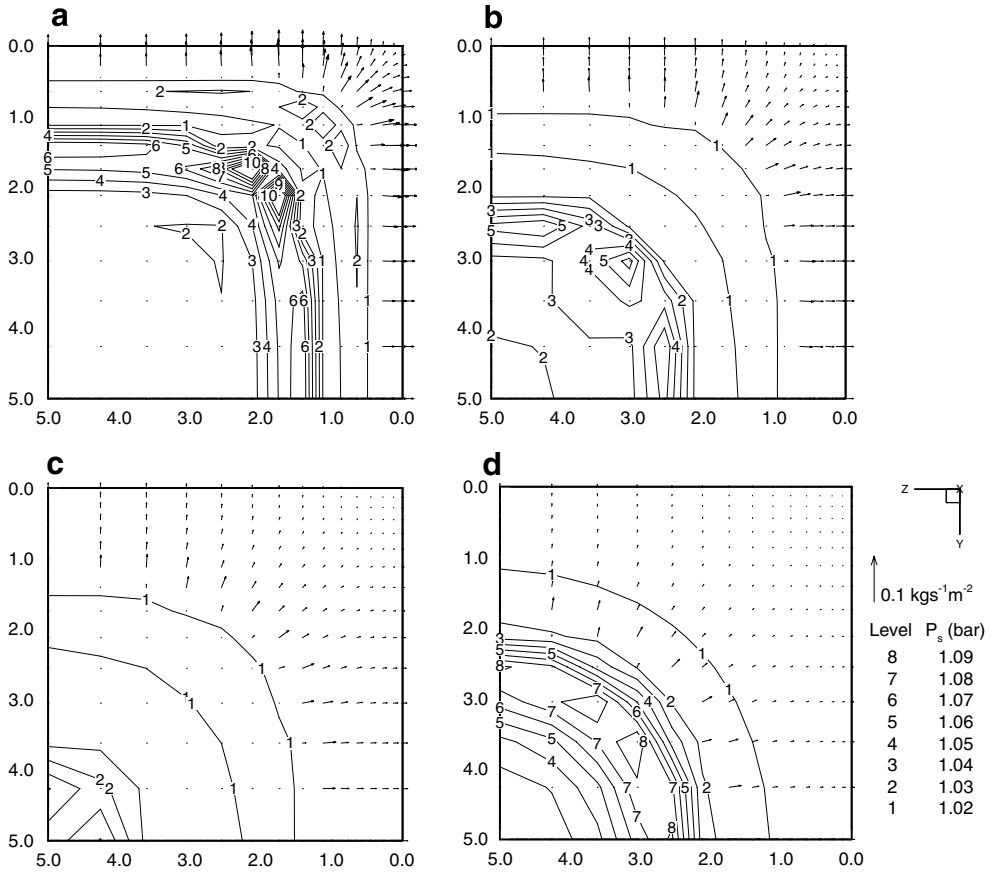


Fig. 12. Contours of total gas pressure and total mass flux vector field on $y$–$z$ plane at $x = 5$ mm (mid-plane) at times: (a) 10 s, (b) 20 s, (c) 30 s and (d) 40 s for $T_f = 1273$ K and $X_0 = 9\%$.

corresponding to the evaporation of moisture reaches the centre of cube and the evaporation in wood is complete after 50 s.

The total mass flux vectors indicating the magnitude and directions of flows of gases and vapour represent the resultant fluxes in $y$- and $z$-directions. Initially, at $t = 10$ s and $t = 20$ s, significant outflows are found at the top and left edge of the wood when the high-pressure zones are still close to these edges. As the high-pressure zones move deeper towards the centre of the wood, these outflows decrease gradually in magnitude because of the less favorable movement of the gases and vapour in the $y$- and $z$-directions where the permeabilities are lower (i.e. across the grains). In fact, the $x$-direction along the grains, where the permeability is much higher, is the prevailing direction of flow at all times.

Fig. 11 represents the isobars and the total mass flux vector field from $t = 10$–40 s for the furnace temperature of 1273 K, on the $x$–$z$ plane at $y = 5$ mm (mid-plane) cutting parallel to the direction of grains. Similarly, the two pressure zones (which correspond to the evaporation and devolatilisation) are identified from $t = 10$–30 s. The two pressure zones move to the left towards the centre of the cube. Upon completion of evaporation, only the pressure zone due to devolatilisation is observed. Two peak outflows corresponding to the vapour and gases are found predominantly at the top edge of the cube as in the case with furnace temperature of 973 K discussed previously. They migrate laterally to the left following the pressure zones.

Fig. 12 shows the isobars and the total mass flux vector field from $t = 10$–40 s for same furnace as above, but on the $y$–$z$ plane at $x = 5$ mm (mid-plane) cutting perpendicular to the direction of grains. The isobars and mass flux vector fields are symmetrical about the diagonal line from the origin of the computational domain. The behaviours of the isobars and mass flux vector field are found similar to that of the case of furnace temperature 973 K as discussed above.

## 6. Conclusion

A 3-D mathematical model for the pyrolysis of wet wood has been developed which includes detailed considerations of the evaporation of moisture, anisotropic and variable properties, and pressure driven internal convection of gases in wood. Although a single first-order Arrhenius reaction is modelled, multiple competing reactions for up to six constituents have been formulated in the computational code. The governing equations have been transformed into a non-orthogonal curvilinear coordinate system, making the model applicable to a large range of geometries.

The system of governing equations has been solved numerically using a control volume technique to predict the pyrolysis of a beech wood cube with different initial moisture contents heated at various furnace temperatures. The activation energy of 125 kJ mole$^{-1}$ and pre-exponential factor of $1.25 \times 10^8$ s$^{-1}$ for the pyrolysis reaction of the single constituent has been determined by achieving a best fit to the measured mass loss history reported by Bonnefoyet al. [25]. These values are in good agreement with the range of kinetic data previously reported [8]. The pre-exponential factor is, however, higher than the reported value in [25] because accounting the presence of moisture evaporation in the current model. This demonstrates the need for a detailed consideration of moisture evaporation for a precise representation of the pyrolysis of hygroscopic material such as wood.

A set of computed results for the pyrolysis of a wet wooden cube with an initial moisture of 9% heated at a furnace temperature of 973 K and 1273 K giving a 3-D quantitative description of the transient processes has been selected and presented in this paper. The transient development and distribution of the temperature, pressure, gas and vapour flow, moisture evaporation and char fraction for different furnace temperatures are reported. The influences of the anisotropic properties due to the grain structure on the heat and mass transfers in pyrolysing wood are discussed. The results significantly showed the faster and earlier evaporation of moisture in the direction along the grains due to the higher permeabilities along the grains. On the other hand, the rate of heating in this direction is slower due to the convective cooling by vapour and volatile gases and to evaporative cooling.

It has been demonstrated in this paper that the current 3-D model for pyrolysis of wet wood can be used to describe the sophisticated chemical and physical processes involved in wood pyrolysis. As the computational code has been formulated to include multiple competing reactions for the major constituents, these improvements are expected to improve the predictions by making use of this feature in future applications.

## References

[1] C. Di Blasi, Comparison of semi-global mechanisms for primary pyrolysis of lignocellulosic fuels, J. Anal. Appl. Pyrolysis 47 (1998) 43–64.
[2] C. Di Blasi, G. Portoricco, M. Borrelli, C. Branca, Oxidative degradation and ignition of loose-packed straw beds, Fuel 78 (1999) 1591–1598.
[3] C. Di Blasi, C. Branca, A. Santoro, E.R. Hernandez, Pyrolytic behavior and products of some wood varieties, Combust. Flame 124 (2001) 165–177.
[4] C. Di Blasi, C. Branca, Kinetics of primary product formation from wood pyrolysis, Ind. Eng. Chem. Res. 41 (2002) 4201–4208.
[5] M.G. Grønli, G. Várhegyi, C. Di Blasi, Thermogravetric analysis and devolatilization kinetics of wood, Ind. Eng. Chem. Res. 40 (2002) 5547–5556.
[6] C. Branca, C. Di Blasi, Kinetics of the isothermal degradation of wood in the temperature range 528–708 K, J. Anal. Appl. Pyrolysis 67 (2003) 207–219.
[7] F. Jia, E.R. Galea, M.K. Patel, The numerical simulation of the noncharring pyrolysis process and fire development within a compartment, Appl. Math. Modell. 23 (1999) 587–607.
[8] R.K.K. Yuen, G. de Vahl Davis, E. Leonardi, G.H. Yeoh, The influence of moisture on the combustion of wood, Numer. Heat Transfer, Part A: Appl. 38 (2000) 257–280.
[9] C.H. Bamford, J. Crank, D.H. Malan, The combustion of wood: Part I, Proc. Cambridge Philos. Soc. 42 (1946) 166–182.
[10] E.R. Tinney, The combustion of wooden dowels in heated air, in: 10th Symposium (International) on Combustion, The Combustion Institute, 1965, pp. 925–930.
[11] A.M. Kanury, P.L. Blackshear Jr., Some considerations pertaining to the problem of wood-burning, Combust. Sci. Technol. 1 (1970) 339–355.
[12] A.M. Kanury, Thermal decomposition kinetics of wood pyrolysis, Combust. Flame 18 (1972) 75–83.
[13] H.C. Kung, A mathematical model of wood pyrolysis, Combust. Flame 18 (1972) 185–195.
[14] H.C. Kung, A.S. Kalelkar, On the heat of reaction in wood pyrolysis, Combust. Flame 20 (1973) 91–103.
[15] A.F. Roberts, A review of kinetics data for the pyrolysis of wood and related substances, Combust. Flame 14 (1970) 261–272.
[16] S.S. Alves, J.L. Figueiredo, A model for pyrolysis of wet wood, Chem. Eng. Sci. 44 (1989) 2861–2869.
[17] B. Fredlund, A model for heat and mass transfer in timber structures during fire: a theoretical, numerical and experimental study, Report LUTVDG/(TVBB-1003), Lund University, 1988.
[18] B. Fredlund, Modelling of heat and mass transfers in wood structures during fire, Fire Safety J. 20 (1993) 39–69.
[19] C. Di Blasi, On the influence of physical processes on the transient pyrolysis of cellulosic samples, Int. Symp. Fire Safety Sci. (1994) 229–240.
[20] C. Di Blasi, Physico-chemical processes occurring inside a degrading two-dimensional anisotropic porous medium, Int. J. Heat Mass Transfer 41 (1998) 4139–4150.
[21] A.G.W. Bradbury, Y. Sakai, F. Shafizadeh, A kinetic model for pyrolysis of cellulose, J. Appl. Polym. Sci. 23 (1979) 3271–3280.
[22] A. Broido, M.A. Nelson, Char yield on pyrolysis of cellulose, Combust. Flame 24 (1975) 263–268.
[23] C. Di Blasi, Modelling the fast pyrolysis of cellulosic particles in fluid-bed reactors, Chem. Eng. Sci. 55 (2000) 5999–6013.
[24] C. Di Blasi, Modelling intra- and extra-particle processes of wood fast pyrolysis, AIChE J. 48 (2002) 2386–2397.
[25] F. Bonnefoy, P. Gilot, G. Prado, A three-dimensional model for the determination of kinetic data from the pyrolysis of beech wood, J. Anal. Appl. Pyrolysis 25 (1993) 387–394.
[26] H.L. Stone, Iterative solution of implicit approximations of multidimensional partial differential equations, SIAM J. Numer. Anal. 5 (1968) 530–558.